Lawrence Berkeley National Laboratory

Title
Surface Roughness of Stainless Steel Bender Mirrors for Focusing Soft X-rays

Permalink
https://escholarship.org/uc/item/0hr2v5bt

Authors
Yashchuk, Valeriy V.
Gullikson, Eric M.
Howells, Malcolm R.
et al.

Peer reviewed

Surface Roughness of Stainless Steel Bender Mirrors for Focusing Soft X-rays

Valeriy V. Yashchuk, Eric M. Gullikson, Malcolm R. Howells, Steve C. Irick,

Alastair A. MacDowell, Wayne R. McKinney, Farhad Salmassi, and Tony Warwick

Lawrence Berkeley National Laboratory, Berkeley, California, USA

James P. Metz and Thomas W. Tonnessen

InSync Inc., Albuquerque, New Mexico

We have used polished stainless steel as a mirror substrate to provide focusing of soft x-rays in grazing incidence reflection. The substrate is bent to an elliptical shape with large curvature and high stresses in the substrate require a strong elastic material. Conventional material choices of silicon or of glass will not withstand the stress required. The use of steel allows the substrates to be polished and installed flat, using screws in tapped holes. The ultra-high-vacuum bender mechanism is motorized and computer controlled. These mirrors are used to deliver focused beams of soft x-rays onto the surface of a sample for experiments at the Advanced Light Source (ALS). They provide an illumination field that can be as small as the mirror demagnification allows, for localized study, and can be enlarged, under computer control, for survey measurements over areas of the surface up to several millimeters. The critical issue of the quality of the steel surface, polished and coated with gold, which limits the minimum achievable focused spot size is discussed in

detail. Comparison is made to a polished, gold coated, electroless nickel surface, which provides a smoother finish. Surface measurements are presented as power spectral densities, as a function of spatial frequency. The surface height distributions measured with an interferometric microscope, and complemented by atomic force microscope measurements, are used to compute power spectral densities and then to evaluate the surface roughness. The effects of roughness in reducing the specular reflectivity are verified by soft x-ray measurements.

OCIS codes

1. Introduction

Shaped mirrors are commonly used in pairs[1-20] for focusing x-rays into experiments at Synchrotron Radiation facilities. These mirrors typically reflect horizontally and vertically, each focusing in one plane. They are often used at high de-magnification to generate a small x-ray spot and tangentially should have an elliptical surface. Bending mechanisms for this type of mirror have been extensively studied.[21-25] They must provide a tuned bending couple at each end of the mirror substrate. This would give a linear variation of curvature from one end of a uniform substrate to the other. The required correction to achieve an elliptically bent shape is generated by varying the width (or thickness) of the substrate as a function of its length. The effects of gravity can be made negligible by a second iteration of this variation.[15] The resulting optical systems have been reported to deliver illumination spots limited by the polished quality of the

substrate.[15] If they are used at short working distances the x-ray spot can be smaller than 1 μm.[26] To keep the mirrors short, they should be used with grazing angles as large as the x-ray reflectivity will allow. For soft x-rays with energy below 2 keV the grazing angle may be 1.5° or larger. An undulator beam can easily be collected at the end of a typical 30 m soft X-ray beamline by a mirror 300 mm long. The required bending radii may be as small as 20 m and the stresses then exceed the capabilities of conventional glass and silicon substrates. Metal is preferred, both for its strength, and for its ease of attachment, in systems that must be baked for ultra-high vacuum and must necessarily be ultra-clean. We have used copper in the past,[15] with an electroless nickel surface for smooth polishing. Stainless steel is stronger and can be polished directly. However, it is not clear, how smooth the finished steel surface can be. These mirrors require an optical coating, usually gold or platinum, but at the proper thickness this coating conforms to the finish and figure of the underlying polished surface.

In this paper we report on the finish achieved on a suite of three stainless steel mirrors recently installed at beamline 11.0.1 at the ALS. The mirror surface roughness was higher than desired, but the mirrors were smooth enough for successful installation and use. One of these three steel mirrors was coated with electroless nickel after the steel failed to polish sufficiently smooth. This extra production step provided a surface that could be polished smooth while retaining the strength of the underlying steel. We show measurements of roughness, scattering, and reflectivity, both from gold-coated polished stainless steel and from gold-coated polished electroless nickel and report on the performance of the benders and the ultimate properties of the x-ray spot at the focus of the beam line.

2. Bender mechanism and substrate stress

Here we discuss one of the three mirrors, focusing with a large demagnification factor of 43 and a working distance 0.5 m. Figure 1 shows the required surface curvature. The dashed line is the best fit with two tunable couples. The desired elliptical shape is then achieved by varying the width of the mirror along its length. Figure 2 shows the bender mechanism with the substrate in place. The substrate is 17-4PH stainless steel, 350 mm long, 50 mm wide, and 20 mm thick. The 7 mm stainless steel (17-4PH) main spring has a deflection $Wl^3/(3EI)$ with $I = wt^3/12$. (W is the pulling force, up to 1000N. w, t and l are the width, thickness and length along the substrate, E is the elastic modulus of the material). The deflection at the end of the spring is about 7 mm. The maximum stress at the fixed end $Wlt/(2I)$ is 4.5×10^8 Nm^{-2} (or 60 ksi). This is just acceptable, as the practical limit against plastic deformation is around 90 ksi. The mirror stress is one fifth of this. The use of 17-4PH stainless steel for the mirror substrate ensures that the polished shape (flat) converts properly into an ellipse even when stressed at this level.

3. Measured surface roughness

The surface roughness measurements were performed with two different instruments and techniques available at the Lawrence Berkeley National Laboratory (LBNL). An interferometric microscope (Micromap-570[27]) with five inter-changeable objectives (2.5×, 5×, 10×, 20×, and 50×) at the ALS Optical Metrology Laboratory (OML) covers a range of spatial frequencies from $4 \cdot 10^{-4}$ µm^{-1} to 2 µm^{-1} (see section 3.1). An Atomic Force Microscope (AFM) (Digital Instruments 3100[28] at the Center for X-Ray Optics (CXRO) Nano-Fabrication facility provides

investigation of the mirror surface finish over an area from 5×5 μm^2 to 100×100 μm^2, covering the spatial frequency range from approximately 0.1 μm^{-1} to 50 μm^{-1} (see section 3.2). For a more sophisticated characterization of the mirror finishes, the surface height distributions measured with these microscopes were transformed into two-dimensional (2D) power spectral density (PSD) functions.[29] The roughness values were estimated based on the obtained 2D PSD distributions.

X-ray reflectivity and scattering measurements were performed at the CXRO Reflectometry and Scattering beamline 6.3.2 at the ALS. Such measurements can also be converted into PSD spectra for the spatial frequency range from 0.1 μm^{-1} to 100 μm^{-1} for 100-1000 eV x-rays.[30,31] This frequency range almost coincides with the AFM range. At the lower frequencies, 0.1 μm^{-1} to 2 μm^{-1}, the range overlaps with the Micromap-570 interferometric microscope measurements. It is possible to cross-check these PSD measurement techniques and eliminate the effects related to the modulation transfer function (MTF) of the instruments.

A 2D PSD function is a Fourier decomposition of the two-dimensional surface height distribution into harmonic basis functions.[29] Its use is preferred to the characterization of the surface finish by the parameters of rms roughness and correlation length.[32] X-ray scattering calculations based on a 2D PSD can be used to reliably evaluate in-plane and out-of plane distributions of the X-rays scattered by the optics; whereas, due to the dependence of the rms roughness and correlation length parameters on the instrumental bandwidth, the corresponding scattering calculation is less reliable and only the evaluation of the integrated scattering can be performed.

A. Interferometric microscope measurements

The Micromap-570 interferometric microscope is a basic metrology tool for measuring micro-roughness of X-ray optics. The instrument in the LBNL OML has demonstrated measurements of sub-angstrom surface roughness. The measurement is in the form of a height distribution on a two-dimensional surface grid that sets the maximum spatial frequency consistent with the magnification number of the objective used for measuring. A number of available objectives with magnification from 2.5× up to 50× allows for measuring roughness over a spatial frequency range from $4 \cdot 10^{-4} \, \mu m^{-1}$ to $2 \, \mu m^{-1}$. In order to suppress instrumental errors, the measurements were performed in "super smooth mode". In this mode, an output height distribution $h_{m,n}$ is the result of two successive measurements over two different regions on the surface. The indices m and n count the pixels. The measured height distributions are subtracted one from another and renormalized in order to preserve the rms roughness (dispersion) of the resulting surface to be equal to the surface roughness of a single measurement:

$$h_{m,n} = \left(h_{1\,m,n} - h_{2\,m,n} \right) / \sqrt{2} \, .$$

The standard output of the Micromap-570 includes the values of roughness averaged over a specified area and averaged along a specified line. However, the two dimensional distribution of the surface height contains more information about the quality of the surface, and can be used to derive a PSD distribution. The procedure and the software developed for converting the 2D surface height distribution measured with the Micromap-570 into a 2D PSD distribution are described elsewhere.[33] Here we present the basic relations necessary for further consideration.

The 2D PSD function S_2 may be viewed as a Fourier decomposition of the 2D surface height distribution $h(x,y)$ into harmonic basis functions:[34]

$$S_2(u,v) = \lim_{A \to \infty} \left\langle \frac{1}{A} \left| \int_{-L_y/2}^{L_y/2} dy \int_{-L_x/2}^{L_x/2} h(x,y) \, e^{-i2\pi(sux+svy)} dx \right|^2 \right\rangle, \tag{1}$$

where L_x and L_y are the tangential and sagittal dimensions of the measured surface region, $A = L_x L_y$; u and v are the spatial frequency variables corresponding to the tangential x and sagittal y coordinates. In the case of discreet measurements with pixel dimensions Δx and Δy, M and N pixels in the tangential and sagittal directions respectively, the 2D PSD distribution can be evaluated from the height distribution $h_{m,n}$ via equation

$$S_2(l,k) = M \, N \, \Delta x \, \Delta y \left| F_{l,k} \right|^2, \tag{2}$$

where $F_{l,k}$ are the elements of the Fourier transform matrix

$$F_{l,k} = \frac{1}{M} \sum_{m=0}^{M-1} \left[\exp\left(\frac{-2\pi i \, m \, l}{M} \right) \frac{1}{N} \sum_{n=0}^{N-1} h_{m,n} \exp\left(\frac{-2\pi i \, n \, k}{N} \right) \right]. \tag{3}$$

The corresponding estimates of the tangential and sagittal one-dimensional (1D) two-sided PSDs $S_1'(l)$ and $S_1'(k)$ can be obtained by summing over rows (k) or columns (l), respectively. Here $0 \le l \le M-1$ and $0 \le k \le N-1$, and prime signifies a two-sided PSD. These are then converted to one-sided (positive frequency only) just like the ones calculated from lines on the surface directly

$$S_1(l) = 2 S_1'(l) g(l) \text{ and } S_1(k) = 2 S_1'(k) g(k), \tag{4}$$

where $0 \leq l \leq M/2$, $0 \leq k \leq N/2$; $g(l) = 1/2$ at $l = 0, M/2$, $g(k) = 1/2$ at $k = 0, N/2$, and $g(l) = 1$ and $g(k) = 1$ otherwise. The reader is directed to reference[33] where the details of the procedure are given.

In order to transform the area distribution of the residual surface heights available from the measurement with the Micromap-570 into a 2D PSD distribution of the surface height, a measured 2D height distribution is first detrended with a best-fit 2D toroidal surface. The general expression for the toroidal surface is given by the expression:

$$S(x,y) = k_{00} + k_{10}x + k_{20}x^2 + k_{01}y + k_{02}y^2 + k_{11}xy + k_{21}x^2y + k_{12}xy^2 + k_{22}x^2y^2. \tag{5}$$

Second, correction for the resolution asymmetry of the Micromap-570 interferometric microscope between the tangential and sagittal directions is performed. This asymmetry originates from the CCD camera read-out through two independent channels with unbalanced amplification. In order to eliminate the related distortion of measured height distributions, the usual practice is to average the height distribution over two adjacent pixels in the sagittal direction. This averaging leads to a resolution asymmetry in the instrument, which is clearly seen when comparing the tangential and sagittal 1D PSD spectra of a mirror with isotropic finish. The asymmetry correction, based on a simple one-parameter analytical model,[33] allows us to account for the major effect of the averaging in the sagittal direction.

The dependence of instrument sensitivity on spatial frequency, which is usually characterized by a Modulation Transfer Function (MTF),[35] leads to distortion of the measured PSD distribution compared with the PSD distribution intrinsic to the surface. Such a distortion is seen in a 1D PSD spectrum as a high frequency roll-off (see Fig. 3). The PSD data presented

throughout the present section are not corrected for this effect. In section 4, comparison of the PSD measurements, using the different techniques is shown to provide a method for finding the MTFs of the corresponding instruments. The effectiveness of the procedure developed for PSD presentation of the Macromap-570 measurements has also been demonstrated in Refs.[33,36] with a number of different X-ray optics including mirrors and a grating.

We should mention that the correction implemented leads to hook-like artifacts in the corrected 1D PSD spectra appearing at highest spatial frequencies (see Fig. 3). For practical purposes these artifacts can be ignored, because of their very small magnitude (they are noticeable in Fig. 3 due to a log-log scale). It should be noted that a similar artifact was encountered in the early development of phase-shifted Fizeau interferometers. Special methods for calibration of the modulation transfer function were proposed.[37] Unfortunately, no investigation of the origin of the artifact was reported.

Finally we reproduce the expressions giving the surface rms roughness values from the tangential and sagittal 1D PSDs

$$R_x = \left[\sum_{l=0}^{M/2} S_1(l) \Delta f_x \right]^{1/2} \quad \text{and} \quad R_y = \left[\sum_{k=0}^{N/2} S_1(k) \Delta f_y \right]^{1/2} . \tag{6}$$

In (6), Δf_x and Δf_y are corresponding spatial frequency intervals, $\Delta f_x = 1/(M \Delta x)$ and $\Delta f_y = 1/(N \Delta y)$. Note that the expressions (6) differ from an analogous formula in Ref.[29] by factor of $\sqrt{2}$. The difference is due to the difference between definitions of the 1D PSD distributions as two-sided 1D PSD used in Ref.[29] and as one-sided 1D PSD given by (4).

Figure 3 shows an example of the 1D PSD spectra extracted from the 2D PSD distribution of the nickel coated steel mirror measured with the Micromap-570 with the 20×

9

objective. The spectra are averaged over measurements of five different regions of the mirror surface. The close similarity of the tangential and sagittal 1D PSD spectra presented in Fig. 3 is a characteristic property of the three stainless steel mirrors: M103 with a nickel coating, M104 and M105 without (we adopt the mirror labeling used on the corresponding ALS beamline). The isotropic mirror surface finish is observed using all objectives on the Micromap-570, as well as with the AFM (see section 4). The tangential 1D PSD spectra of the nickel coated steel mirror, measured with different Micromap-570 objectives, are presented in Fig. 4. Each spectrum is the result of a convolution of the corresponding averaged 2D PSD distribution. The 2D PSD measurements with different objectives extend the available spatial frequency range. A noticeable feature of such an extension is that the higher spatial frequency roll-off observed with a lower resolution objective is corrected when measuring with a higher resolution objective.

Compared to the nickel coated steel mirror, the 1D PSD spectra measured for the mirrors with stainless steel substrates polished directly have systematically larger magnitudes (see Fig. 5 and Fig. 6). The difference between the 1D PSD spectra of the two mirrors with stainless steel substrates polished directly is significantly smaller.

Table 1 summarizes the result of the Micromap-570 measurements on the mirrors with the stainless steel substrates polished directly in the term of rms surface roughness S_q, which is the standard deviation of the height values of the measured area from the best fit second order polynomial surface. The values of the roughness presented in the table are the Micromap-570 output parameters generated with the instrument's software.

B. Atomic force microscope measurements

The surface finish of two of the mirrors was investigated using an Atomic Force Microscope at the LBNL CXRO Nano-Fabrication facility. These measurements were made on the nickel coated steel mirror and on one of the mirrors with a stainless steel substrate polished directly. A series of AFM scans were performed using a Digital Instruments 3100 instrument with the NanoScope software.[28] The AFM instrument operates with an atomically sharp tip oscillating at resonance above the surface to be measured. The amplitude of the oscillation is adjusted to bring the maximum excursion close to the surface, as the tip is raster-scanned over the region of interest. By reflecting laser light off the back of the tip-cantilever and into a detector system, the AFM instrument is able to resolve sub-nanometer changes in oscillation amplitude corresponding to changes of the height of the surface. Ordinary etched silicon cantilever tips with 15 nm to 20 nm tip diameters were used with response frequencies of approximately 290kHz. The AFM provides surface height distributions that can be converted, with the built-in software, into 1D PSD spectra and 2D PSD distributions. The instrument allows PSD measurements for the spatial frequency range approximately from 0.1 μm^{-1} to 50 μm^{-1}, which correspond to a measuring surface area of up to 100×100 μm^2 with 512×512 elements. In order to produce an accurate characterization of the entire mirror surface, multiple measurements were carried out over different surface regions and averaged PSD spectra were calculated (see Fig. 7). The 1D PSD spectra measured on the M104 mirror with a stainless steel substrate polished directly are plotted in Fig. 8. These data were obtained in just a single measurement over each of the regions. As a result, the spread of data is increased. The lowest spatial frequency artifacts in the 1D PSD spectra measured with this mirror are due to the detrending procedure with subtraction of a residual surface described by a third-order polynomial. Table 2 summarizes the result of the AFM measurements with the two mirrors in

terms of the rms surface roughness S_q. The values of the roughness presented in the table are the AFM output parameters generated with the instrument's software.

C. X-ray scattering and reflectivity

The X-ray scattering and reflectivity measurements were performed with the Reflectometry and Scattering beamline 6.3.2[38,39] at the ALS. The scattering measurements can be converted into the PSD spectra for the spatial frequency range from 0.1 μm^{-1} to 100 μm^{-1} for 100-1000 eV X-rays.

Figure 9 shows the reflectivity versus angle at 92 eV for the directly polished stainless steel mirror M104. The smooth-surface reflectivity is shown by the dashed line, while the solid line is a fit to the data using a Nevot-Croce factor and a roughness of 1.8 nm. Figure 10 shows measured reflectivity for the M104 steel mirror and the M103 nickel coated steel (both gold-coated). The reflectivity versus energy of the stainless steel mirror follows very closely the theoretical reflectance curve of the Nevot-Croce model and with an rms roughness of 2 nm consistent with the measurement of figure 9. The measured reflectivity of the Ni coated steel mirror is close to that of a smooth surface. Note that with a high quality surface finish such as that found on the nickel coated steel mirror, the reflectance measurement is rather insensitive to the surface roughness.[40]

The rms roughness deduced from the reflectivity measurements describes the reflectance loss due to x-rays scattered out of the acceptance of the detector. It is therefore related to the high spatial frequency roughness. The exact frequency range depends on the incident angle, the angular acceptance of the detector and the photon energy. For example at 500 eV, integrating

the PSD of the M104 mirror over the frequency range which scatters light out of the 1.2-degree half angle detector acceptance gives an rms roughness of 21 Å consistent with the value obtained from the reflectivity measurements.

The angle dependent scattering was measured for the M104 mirror with a stainless steel substrate polished directly. Scattering measurements were performed at X-ray beam incidence angles of 1.5° and 5° and photon energy of 92 eV. The PSD spectra deduced from the scattering measurements on the M104 mirror are shown in Fig. 11.

4. Power-law approximation of measured PSD distributions

Figures 12 and 13 present the 1D PSD spectra obtained from the polished nickel mirror M103 and from the directly polished steel mirror M104, respectively. The measurements performed with the three different techniques are shown. The AFM spatial frequency range almost coincides with the frequency range of the X-ray scattering experiment. It also overlaps at the lower frequencies with the Micromap-570 interferometric microscope measurements. This allows for crosschecking the techniques.

The main conclusion from the crosscheck is that all three techniques provide essentially consistent results. Moreover, for both mirrors the PSD spectra in the range of spatial frequencies from $3 \cdot 10^{-4}$ µm^{-1} to 10 µm^{-1} can be approximated with a power-law dependence, which is a straight line in the log-log scale used in Figs. 12 and 13. The same power-law approximation has been found to be applicable to the PSD spectra of the high quality X-ray mirrors made of polished glass-ceramics (SiC) and metals.[41,42]

The power-law approximation has two parameters, spectral intensity $S_1(1)$ and spectral index γ,

$$S_1(f_x) = \frac{S_1(1)}{f_x^{\gamma}}, \tag{6}$$

where f_x is the tangential spatial frequency, and index *1* is used to emphasize that $S_1(f_x)$ is 1D PSD function; $S_1(1)$ is a constant equal to $S_1(f_x)$ at $f_x = 1$ μm⁻¹. The power-law parameters found for the mirrors measured here are presented in Table 3. The values of the parameters are given assuming that all dimensional quantities are expressed in microns, $[S_1(f_x)] = $μm³, $[f_x] = $μm⁻¹.

The spectral indexes found for the mirrors under investigation in the present work are too small to be consistent with the concept of fractal surface finish.[18] A fractal profile (with spectral power between one and three) has statistical properties that stay the same under scaling along the surface by a factor ξ and under scaling of height by a factor $\xi^{(\gamma-1)/2}$. This can be thought of as an absence of internal length scales for the fractal profile determined by the polishing process.[18] In our case, the investigated spatial frequency range extends to frequencies high enough that the scale of the polishing process is important, leading to spectral indices smaller than one.

For the inverse-power-law-like surfaces with parameters given in Table 3, the roughness values can be calculated from the corresponding discrete 1D PSD spectrum with Eq. (6). The result of such calculation for the frequency interval and range corresponding to the Micromap measurements with the 5× objective are presented in Table 3. The roughness values shown in Table 3 have a good agreement with the magnitudes presented in Tables 1 and 2. However, the results in Table 3 are considered significantly more reliable, because of the correction of the error due to the instrumental MTF.

5. Conclusions

In the present work, we have shown that surface finish of the stainless steel mirror is significantly improved if, instead of a directly polished steel surface, an additional layer of nickel is applied and polished. The investigation is based on measured power spectral density spectra over a broad range of spatial frequencies from $3 \cdot 10^{-4}$ μm^{-1} to 10 μm^{-1}, available with three different experimental instruments. The instruments are the Micromap-570 interferometric microscope, the Digital Instruments 3100 atomic force microscope, and an experimental facility for measuring X-ray scattering and reflectivity. With all three mirrors investigated, the instruments provide essentially consistent results.

It was demonstrated that a power-law-like topography gives a good approximation for the measured PSD spectra over the broad range of spatial frequencies between $\sim 3 \cdot 10^{-4}$ μm^{-1} to 10 μm^{-1}. The spectral index parameters, characterizing the power-law-like envelopes of the experimental PSD spectra were found to be smaller than one. One is the lower limit for the application of a fractal-like description of the highly polished surface.[32] This can be thought of as a manifestation of a length scale related to the polishing process at very high spatial frequencies.

The parameters found for the power-law approximation were used to obtain the values of the surface roughness, free of errors due to the instrumental modulation transfer functions. The roughness of the polished nickel surface was evaluated to be about 6.4 Å, smaller by factor of approximately two compared to the directly polished stainless steel surface. This improvement decreases the scattering of X-rays, as demonstrated with the X-ray reflectivity experiments described in Sec. 3.

We also emphasize that the AFM and X-ray scattering measurements, which offer higher spatial resolution than measurements with the interferometric microscope, can be used to

determine the Micromap-570 modulation transfer function and can be used to correct the high frequency roll-off of the instrument.[36]

6. Acknowledgements

References

1. Bianco, A., G. Sostero, and D. Cocco, "Kirkpatrick-Baez elliptical bendable mirrors at the nanospectroscopy beamline: metrological results and x-rays performance," in *X-Ray Mirrors, Crystals, and Multilayers II*, Proc. SPIE **4782**, 74-85 (2002).

2. S. J. Chen, C. K. Kuan, S. Y. Perng, D. J. Wang, H. C. Ho, T. C. Tseng, Y. C. Lo, C .T. Chen, "New focusing mirror system for synchrotron radiation infrared beamlines," Opt. Engineering, **43**(12), 3077-3082 (2004).

3. Y. Dabin, G. Rostaing, O. Hignette, A. Rommeveaux, A. K. Freund, "The present state of Kirkpatrick-Baez mirror systems at the ESRF," in *X-Ray Mirrors, Crystals, and Multilayers I,* A. K. Freund, A. T. Macrander, T. Ishikawa, J. L. Wood, eds., Proc. SPIE **4782**, 235-245 (2002).

4. A. K. Freund, "Recent progress in x-ray optics at the ESRF," J. de Physique IV **104,** 165-170 (2003).

5. A. Freund, "Challenges for synchrotron X-ray optics," in *X-Ray Mirrors, Crystals, and Multilayers I,* A. K. Freund, A. T. Macrander, T. Ishikawa, J. L. Wood, eds., Proc. SPIE **4782**, 1-11 (2002).

6. P. A. Heimann, H. A. Padmore, A. A. Zholents, "X-ray optical designs for the Linac-based Ultrafast X-ray source (LUX)," in *Fourth-Generation X-Ray Sources and Ultrafast X-Ray Detectors*, R. O. Tatchyn, Z. Chang, J.-C. Kieffer, J. B. Hastings, eds.*,* Proc. SPIE **5194**, 39-45 (2004).

7. O. Hignette, Cloetens P, W-K. Lee, W. Ludwig, G. Rostaing, "Hard X-ray microscopy with reflecting mirrors status and perspectives of the ESRF technology," J. de Physique IV **104**, 231-234, (2003).

8. G. E. Ice, E. D. Specht, J. Z. Tischler, A. M. Khounsary, L. Assoufid, C. Liu, "At the limit of nondispersive micro- and nanofocusing mirror optics," in *Micromachining Technology for*

Micro-Optics and Nano-Optics II, E. G. Johnson, G. P. Nordin, eds.*,* Proc. SPIE **5347 (**1), 1-8 (2004).

9. M. Janousch, A-M. Flank, P. Lagarde, G. Cauchon, S. Bac, J. M. Dubuisson, Th. Schmidt, R. Wetter, G. Grolimund, A. M. Scheidegger, "LUCIA - a new 1-7 keV mu -XAS beamline," in *Synchrotron Radiation Instrumentation,* T. Warwick, J. Arthur, H. A. Padmore, J. Stöhr, eds., AIP Proceedings, **705**, 312-315 (2004).

10. A. M. Khounsary, G. E. Ice, P.J. Eng, "Mirrors for nanofocusing x-ray beams," in *X-Ray Mirrors, Crystals, and Multilayers II,* A. K. Freund, A. T. Macrander, T. Ishikawa, J. L. Wood, eds., Proc. SPIE **4782**, 65-73 (2002).

11. P. P. Naulleau, P. Batson, P. Denham, D. Richardson, J. Underwood, "An in situ scanning-slit alignment system for Kirkpatrick-Baez optics," Opt. Commun. **212**(4-6), 225-233 (2002).

12. N. A. Papadogiannis, L. A. A. Nikolopoulos, D. Charalambidis, G. D. Tsakiris, P. Tzallas, K. Witte, "On the feasibility of performing nonlinear autocorrelation with attosecond pulse trains," App. Phys. B **76**(7), 721-727 (2003).

13. I. K. Robinson, F. Pfeiffer, I. A. Vartanyants, S. Yugang, X. Younan, "Enhancement of coherent X-ray diffraction from nanocrystals by introduction of X-ray optics," Opt. Express **11**(19), 2329-2334 (2003).

14. R. Spolenak, N. Tamura, B. C. Valek, A. A. MacDowel, R. S. Celestre, H. A. Padmore, W. L. Brown, T. Marieb, B. W. Batterman, J. R. Patel, "High resolution microdiffraction studies using synchrotron radiation," in *Stress-Induced Phenomena in Metallization. Sixth International Workshop on Stress-Induced Phenomena in Metallization,* S. P. Baker, M. A. Korhonen, E. Arzt, P. S. Ho, eds., AIP Proceedings, **612**, 217-228 (2002).

15. T. Warwick, N. Andresen, J. Comins, A. Franck, M. Gilles, T. Tonnessen, T. Tyliszczak, "Large aperture micro-focus KB mirrors for spectroscopy experiments at the Advanced Light Source," in *Synchrotron Radiation Instrumentation,* T. Warwick, J. Arthur, H. A. Padmore, J. Stöhr, eds., AIP Proceedings, **705**, 772-775 (2004).

16. Y. Xiaojiang, H. Zhongwen, P. Haibin, P. Qiuping and X. Pengshou, "The re-design of a soft X-ray beamline for photoemission spectroscopy at NSRL," in *Synchrotron Radiation Instrumentation,* T. Warwick, J. Arthur, H. A. Padmore, J. Stöhr, eds., AIP Proceedings, **705**, 396-399 (2004).

17. K. Yamamura, H. Mimura, K. Yamauchi, Y. Sano, A. Saito, T. Kinoshita, K. Endo, Y. Mori, A. Souvorov, M. Yabashi, K. Tamasaku, T. Ishikawa, "Aspheric surface fabrication in nm-level accuracy by numerically controlled plasma chemical vaporization machining (CVM) and elastic emission machining (EEM)," in *X-Ray Mirrors, Crystals, and Multilayers I,* A. K. Freund, A. T. Macrander, T. Ishikawa, J. L. Wood, eds., Proc. SPIE **4782**, 265-270 (2002).

18. Yamamura, K., K. Yamauchi, H. Mimura, Y. Sano, A. Saito, K. Endo, A. Souvorov, M. Yabashi, K. Tamasaku, T. Ishikawa, Y. Mori, "Fabrication of elliptical mirror at nanometer-level accuracy for hard x-ray focusing by numerically controlled plasma chemical vaporization machining," Rev. Sci. Instrum. **74**(10), 4549-4553 (2003).

19. E. Ziegler, T. Bigault, J. Hoszowska, "An X-ray focusing system combining a sagittally-bent crystal and a Kirkpatrick-Baez system," in *Synchrotron Radiation Instrumentation,* T. Warwick, J. Arthur, H. A. Padmore, J. Stöhr, eds., AIP Proceedings, **705**, 768-771 (2004).

20. Ziegler, E., et al. "The ESRF BM05 metrology beamline: instrumentation and performance upgrade," in *Synchrotron Radiation Instrumentation,* T. Warwick, J. Arthur, H. A. Padmore, J. Stöhr, eds., AIP Proceedings, **705**, 436-439 (2004).

21. J. J. Ferme, "New improvements in bendable mirrors," in *Materials, Manufacturing, and Measurement for Synchrotron Radiation Mirrors*, P. Z. Takacs, T. W. Tonnessen, eds.*,* Proc. SPIE **3152**, 103-111 (1997).

22. Hartman, N.D., et al. "Design, analysis, and performance of an epoxy-bonded bendable mirror," in *Advances in Mirror Technology for Synchrotron X-Ray and Laser Applications,* A. M. Khounsary, eds.*,* Proc. SPIE **3447**, 40-51 (1998).

23. M. R. Howells, "Design strategies for monolithic adjustable-radius metal mirrors," Opt. Eng. **34**(2), 410-17 (1995).

24. E. Morikawa, , J. D. Scott, V. Saile, "Adaptive optics for resolution/throughput optimization; variable-radius-mirror application for a PGM," Nucl. Instr. and Methods **A319**(1-3), 116-120 (1992).

25. Seungyn, R., et al. "New schemes in the adjustment of bendable elliptical mirrors using a Long Trace Profiler," in *Materials, Manufacturing, and Measurement for Synchrotron Radiation Mirrors,* P. Z. Takacs, T. W. Tonnessen, eds., Proc. SPIE **3152**, 112-19 (1997).

26. O. Hignette, et al. "Submicron focusing of hard X-rays with reflecting surfaces at the ESRF," in *X-Ray Micro- and Nano-Focusing: Applications and Techniques II,* I. McNulty, ed., Proc. SPIE **4499**, 105-116 (2001).

27. Micromap Corporation (Tucson, AZ; phone +1 520-881-1911; fax +1 520-881-1913).

28. Digital Instruments/Veeco Instruments Inc., http://www.veeco.com/.

29. J. C. Stover, *Optical Scattering; Measurement and Analysis* (SPIE Optical Engineering Press, Bellingham, 1995).

30. J. V. Bixler, C. W. Mauche, C. J. Hailey, L. Medison, "Reflectivity and scattering measurements of an Advanced X-ray Astrophysics Facility test coating sample," App. Optics **34**(28), 6542-6551 (1995).

31. V. E. Asadchikov, I. V. Kozhevnikov, Yu. S. Krivonosov, R. Mercier, T. H. Metzger, C.Morawe, E. Ziegler, "Application of X-ray scattering technique to the study of supersmooth surfaces," Nucl. Instr. and Methods **A530**, 575-595 (2004).

32. E. L. Church, "Fractal Surface Finish," App. Optics **27**(8),1518-1526 (1988).

33. V. V. Yashchuk, A. D. Franck, S. C. Irick, M. R. Howells, A. A. MacDowell, W. R. McKinney, "Two dimensional power spectral density measurements of X-ray optics with the Micromap interferometric microscope," in *Nano- and Micro-Metrology,* H.Ottevaere, P. DeWolf, D. S. Wiersma, eds., Proc. SPIE **5858**, 85-96 (2005).

34. R. N. Bracewell, *The Fourier Transform and Its Applications* (McGraw-Hill Publishing Company, New York , 1986), pp.108-112.

35. G. D. Boreman, *Modulation Transfer Function in Optical and Electro-optical Systems* (SPIE Press, Bellingham, 2001).

36. V. V. Yashchuk, S. C. Irick, E. M. Gullikson, M. R. Howells, A. A. MacDowell, W. R. McKinney, F. Salmassi, T. Warwick, "Crosscheck of different techniques for two dimensional power spectral density measurements of X-ray optics," in *Advances in Metrology for X-Ray and EUV Optics,* L. Assoufid, P. Z. Takacs, J. S. Taylor, eds., Proc. SPIE **5921**, 105-116 (2005).

37. G. Zhishan, C. Jinbang, "Calibration of Frequency Response Function for a Phase-shifted Interferometer," in *Advanced Optical Manufacturing and Testing Technology 2000*, L. Yang, H. M. Pollicove, Q. Xin, J. C. Wyant eds., Proc. SPIE **4231**, 397-401 (2000).

38. Center for X-Ray Optics, Materials Science Division, Lawrence Berkeley Laboratory, Berkeley, CA; http://www.cxro.lbl.gov/als6.3.2.

39. J.H. Underwood, E. H. Gullikson, "High-resolution, high-flux, user friendly VLS beamline at the ALS for the 50-1300 eV energy region," J. Electr. Spectrosc. and Related Phenom **92**, 265-272 (1988).

40. Gullikson, E., Center for X-Ray Optics; http://www.cxro.lbl.gov/optical_constants/mirror2.html.

41. E. L. Church, P. Z. Takacs, "Surface Scattering," in *Handbook in Optics, Vol. 1: Classical Optics, Vision Optics, X-Ray Optics*, M. Bass, Jay M. Enoch, E. W. Van Stryland, W. L. Wolfe eds., (Second Edition, McGraw-Hill Inc., New York, 2000), Ch. 7.

42. P. Z. Takacs, E. L. Church, "Figure and Finish of Grazing-incidence Mirrors," Nucl. Instr. and Methods **A291**, 253-264 (1990).

Figure captions

Figure 1: Mirror shape required for perfect focusing, expressed as curvature versus length along the substrate. The dashed line is the best fit achievable with a uniform substrate.

Figure 2: Schematic of flange mounted bending mechanism showing motorized drives, spring/pivot components in ultra high vacuum and the mirror substrate to be bent.

Figure 3: 1D PSD spectra extracted from the 2D PSD distribution of the M103 nickel coated steel mirror measured with the Micromap-570 with the 20× objective. The solid line shows the tangential spectrum; the dashed line represents the sagittal spectrum. The spectra are the result of averaging over measurements of five different areas of the mirror surface. The roll-off seen at higher spatial frequencies is due to the modulation transfer function of the microscope. The hook-like features at the highest frequencies are the artifacts of the correction of the CCD camera read-out asymmetry (see text).

Figure 4: 1D PSD spectra extracted from the 2D PSD distribution of the M103 nickel coated steel mirror measured with the Micromap-570 with all available objectives. Each spectrum is the result of averaging over measurements of five different areas of the mirror surface.

Figure 5: 1D PSD spectra extracted from the 2D PSD distribution of the M104 directly polished stainless steel mirror measured with the Micromap-570 with all available objectives. Each spectrum is the result of averaging over measurements of five different areas of the mirror surface.

Figure 6: 1D PSD spectra extracted from the 2D PSD distribution of the M105 directly polished stainless steel mirror measured with the Micromap-570 with all available objectives.

Figure 7: 1D PSD spectra measured with the AFM instrument over different surface area of the M103 nickel coated steel mirror. Each spectrum is a result of averaging over four measurements of different surface spots at the same AFM settings. The AFM measurements are rather consistent while measuring over areas with different size, from $5 \times 5\ \mu m^2$ to $100 \times 100\ \mu m^2$. However, at lower spatial frequencies, the $50 \times 50\ \mu m^2$ and $100 \times 100\ \mu m^2$ area measurements systematically give larger 1D PSD values than the measurements over smaller areas.

Figure 8: 1D PSD spectra measured with the AFM instrument over different surface area of the M104 directly polished stainless steel mirror. The lowest spatial frequency artifacts are due to the detrending procedure with subtraction of a residual surface described with a third power polynomial.

Figure 9: X-ray reflectivity versus angle for the M104 directly polished stainless steel mirror measured at 92 eV. The dashed line shows the theoretical reflectivity of a perfectly smooth mirror and the solid line is a fit to the measurements using a Nevot-Croce factor to model the scattering loss and an rms roughness of 18 Å.

Figure 10: X-ray energy dependences of the surface reflectance measured with the nickel coated steel mirror (the open points) the M104 directly polished stainless steel mirror (the filled points). The solid and the dashed lines represent the theoretical spectra computed from tabulated optical properties of gold, with a Nevot-Croce treatment of the loss due to surface roughness assuming the mirror surface roughness of 5 Å for the nickel coated steel mirror M103 and 20 Å for the directly polished stainless steel mirror, M104. The steel reflectivity is reduced above 200eV by surface roughness effects.

Figure 11: The 1D PSD spectra extracted from the X-ray scattering measurements with the M104 directly polished mirror. The solid line corresponds to the X-ray beam grazing incidence angle of 1.5°; and the dashed line obtained at the beam grazing angle of 5°. The measurements were performed at photon energy of 92 eV.

Figure 12: Tangential 1D PSD spectra obtained with the M103 nickel coated mirror. The spectra at lower spatial frequencies show the measurements with different objectives of the interferometric microscope (compare with Fig. 4); the spectra at higher spatial frequencies represent the Atomic Force Microscope data (compare with Fig. 7). The dashed line represents an inverse-power-low spectrum, enveloping all the measured spectra. Note that the parameters of inverse-power-low spectrum (Table 3) are the same as for the sagittal 1D PSD spectra measured with the Micromap and AFM.

Figure 13: Tangential 1D PSD spectra obtained with the directly polished stainless steel mirror M104. The spectra at lower spatial frequencies show the measurements with different objectives of the interferometric microscope (compare with Fig. 5); the spectra at the middle spatial frequencies represent the Atomic Force Microscope data (compare with Fig. 8); the spectra extracted from the X-ray Scattering measurements cover the higher frequencies available. The dashed line represents an inverse-power-low spectrum, enveloping all the measured spectra. Note that the parameters of the inverse-power-low spectrum (Table 3) are the same as for the sagittal 1D PSD spectra measured with the Micromap and AFM.

Figures

Figure 1: Mirror shape required for perfect focusing, expressed as curvature versus length along

the substrate. The dashed line is the best fit achievable with a uniform substrate.

Figure 2: Schematic of flange mounted bending mechanism showing motorized drives, spring/pivot components in ultra high vacuum and the mirror substrate to be bent.
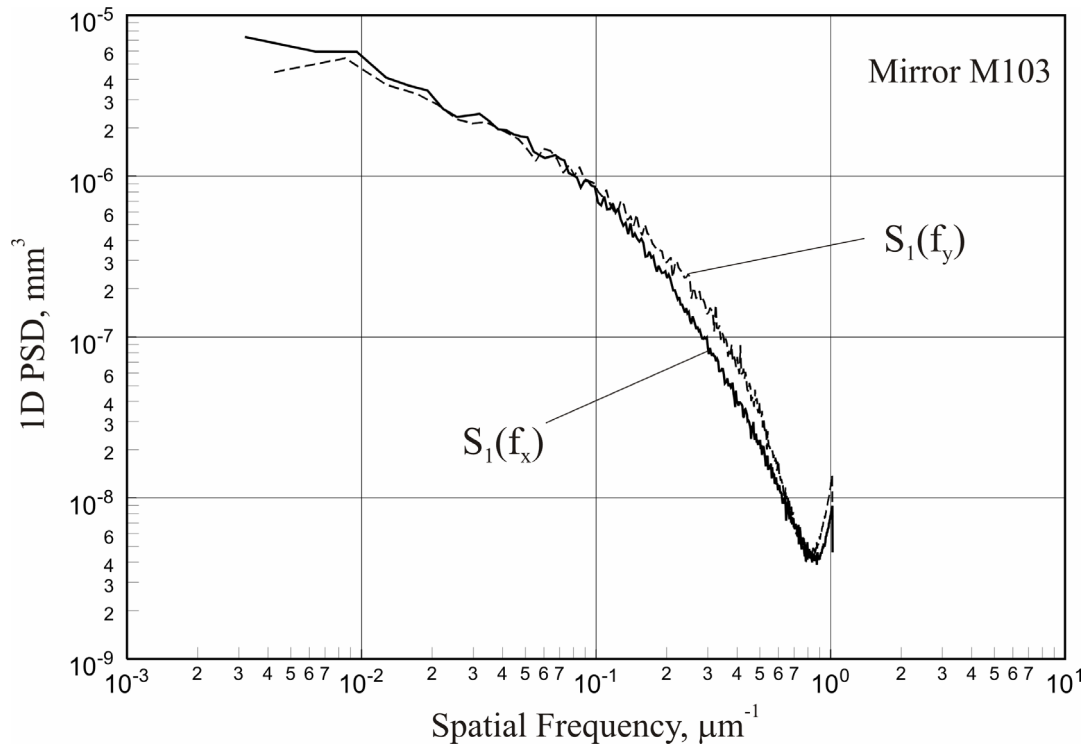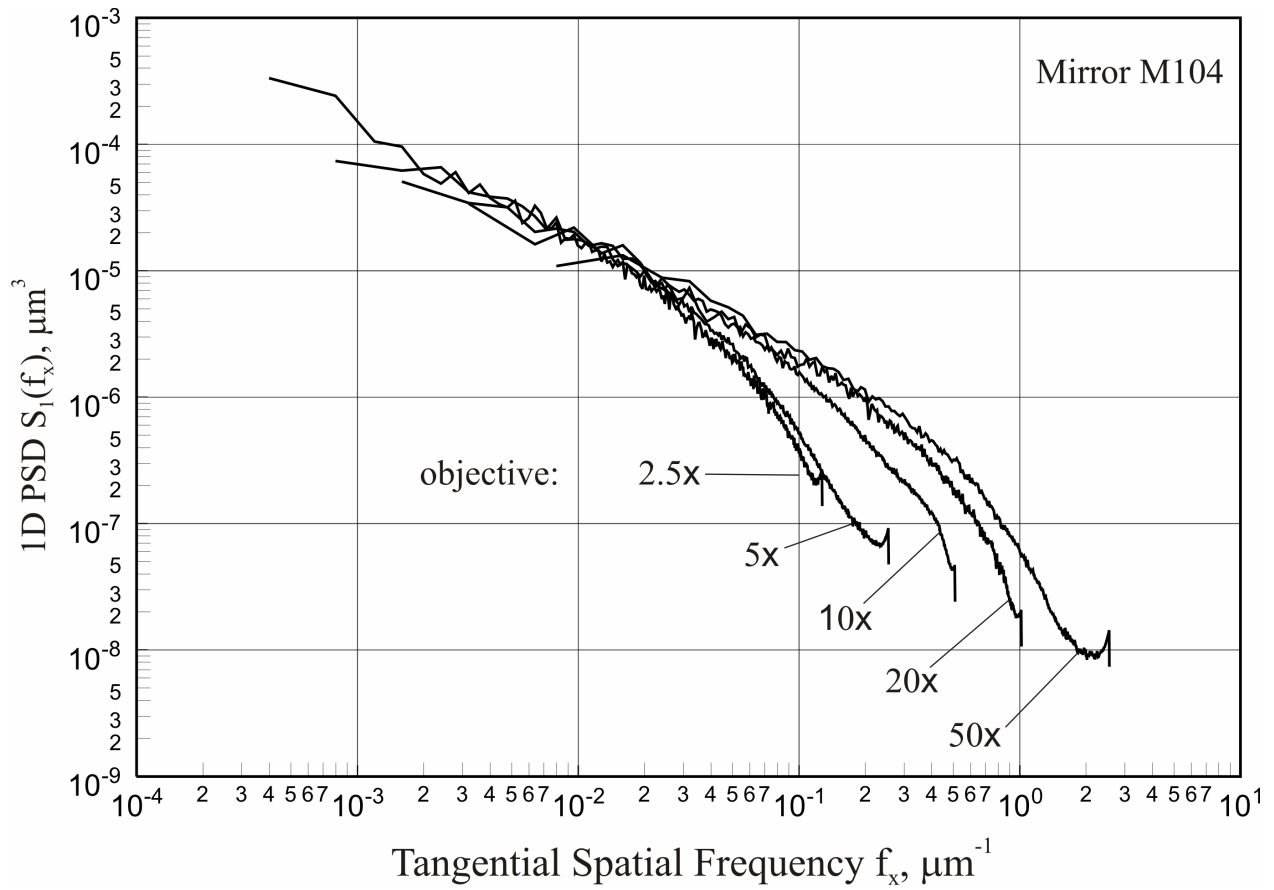
Figure 3: 1D PSD spectra extracted from the 2D PSD distribution of the M103 nickel coated steel mirror measured with the Micromap-570 with the 20× objective. The solid line shows the tangential spectrum; the dashed line represents the sagittal spectrum. The spectra are the result of averaging over measurements of five different areas of the mirror surface. The roll-off seen at higher spatial frequencies is due to the modulation transfer function of the microscope. The hook-like features at the highest frequencies are the artifacts of the correction of the CCD camera read-out asymmetry (see text).

Figure 4: 1D PSD spectra extracted from the 2D PSD distribution of the M103 nickel coated steel mirror measured with the Micromap-570 with all available objectives. Each spectrum is the result of averaging over measurements of five different areas of the mirror surface.
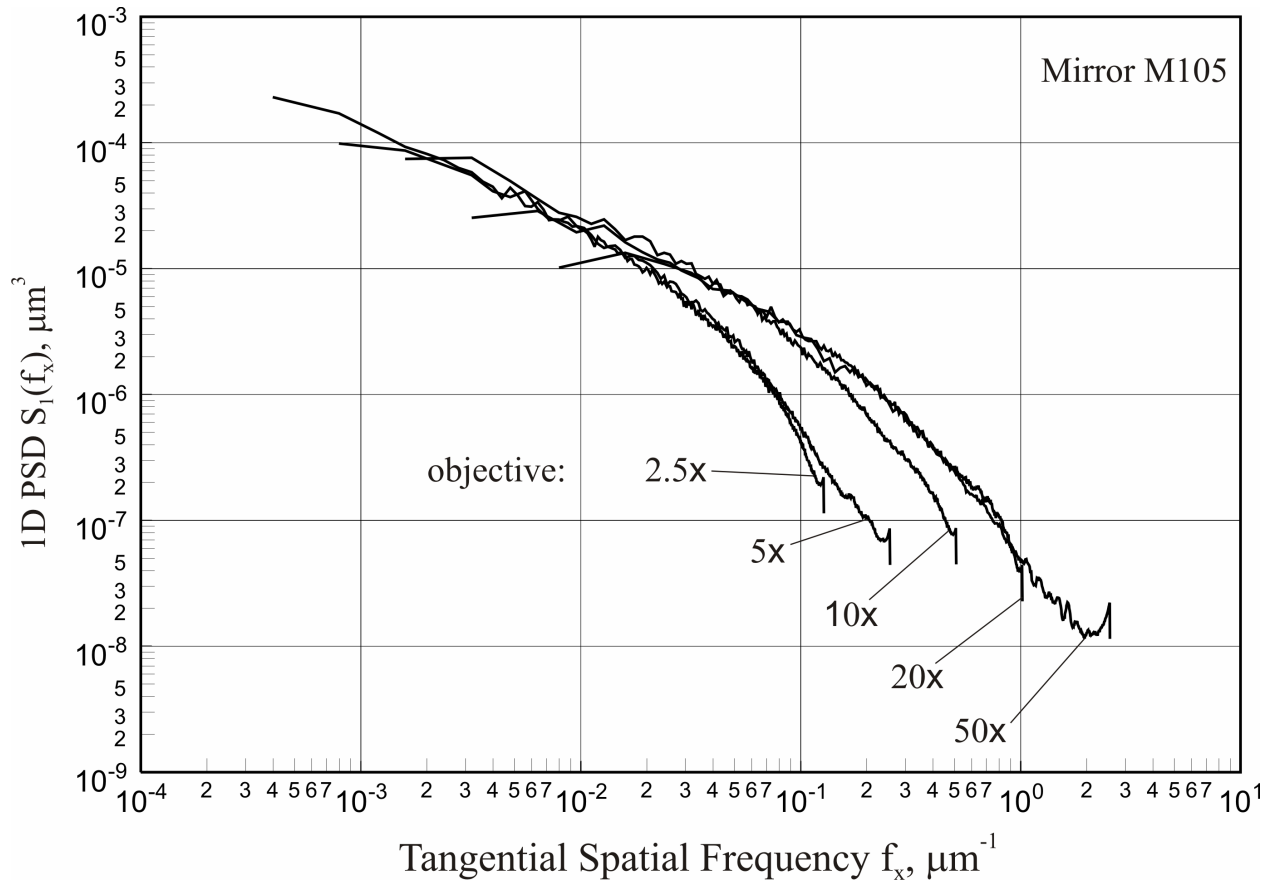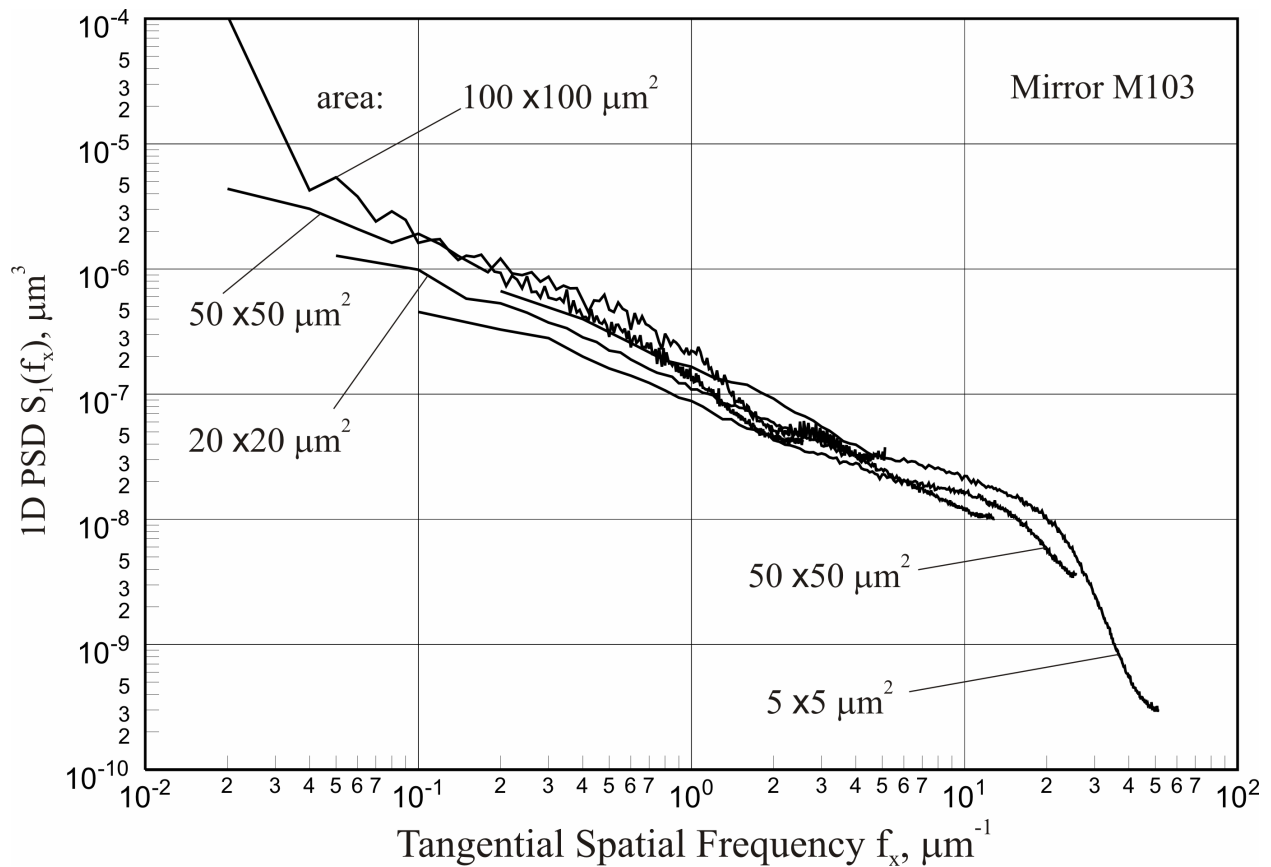
Figure 5: 1D PSD spectra extracted from the 2D PSD distribution of the M104 directly polished stainless steel mirror measured with the Micromap-570 with all available objectives. Each spectrum is the result of averaging over measurements of five different areas of the mirror surface.

Figure 6: 1D PSD spectra extracted from the 2D PSD distribution of the M105 directly polished stainless steel mirror measured with the Micromap-570 with all available objectives.
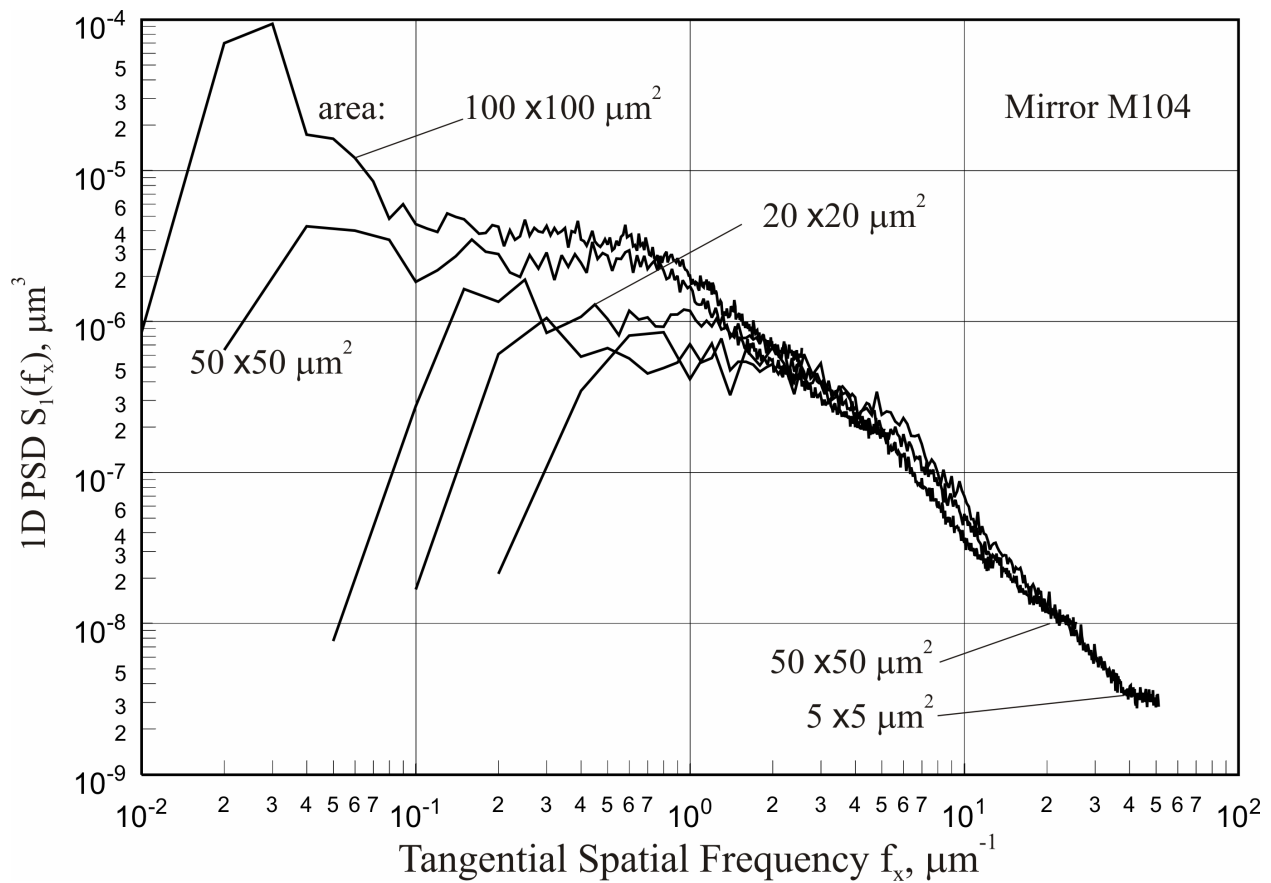
Figure 7: 1D PSD spectra measured with the AFM instrument over different surface area of the M103 nickel coated steel mirror. Each spectrum is a result of averaging over four measurements of different surface spots at the same AFM settings. The AFM measurements are rather consistent while measuring over areas with different size, from $5 \times 5\ \mu m^2$ to $100 \times 100\ \mu m^2$. However, at lower spatial frequencies, the $50 \times 50\ \mu m^2$ and $100 \times 100\ \mu m^2$ area measurements systematically give larger 1D PSD values than the measurements over smaller areas.

Figure 8: 1D PSD spectra measured with the AFM instrument over different surface area of the M104 directly polished stainless steel mirror. The lowest spatial frequency artifacts are due to the detrending procedure with subtraction of a residual surface described with a third power polynomial.
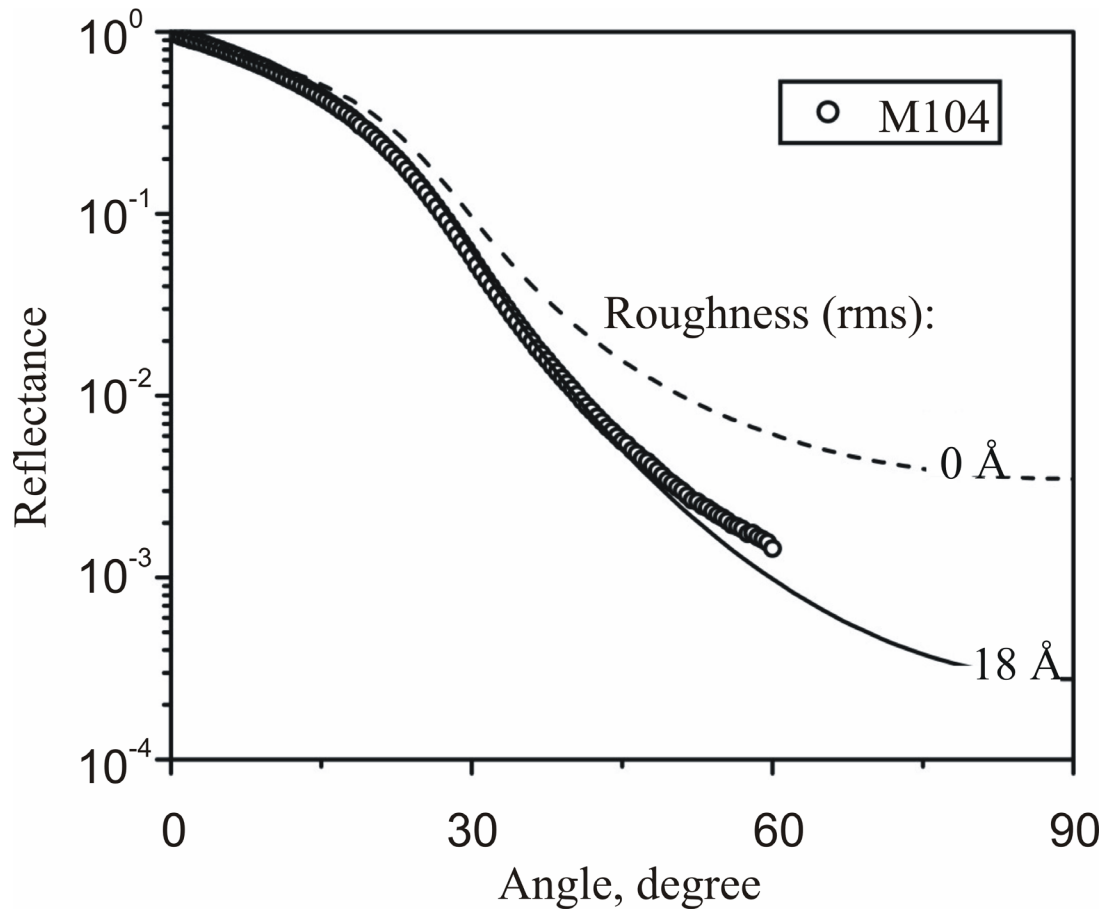
Figure 9: X-ray reflectivity versus angle for the M104 directly polished stainless steel mirror measured at 92 eV. The dashed line shows the theoretical reflectivity of a perfectly smooth mirror and the solid line is a fit to the measurements using a Nevot-Croce factor to model the scattering loss and an rms roughness of 18 Å.
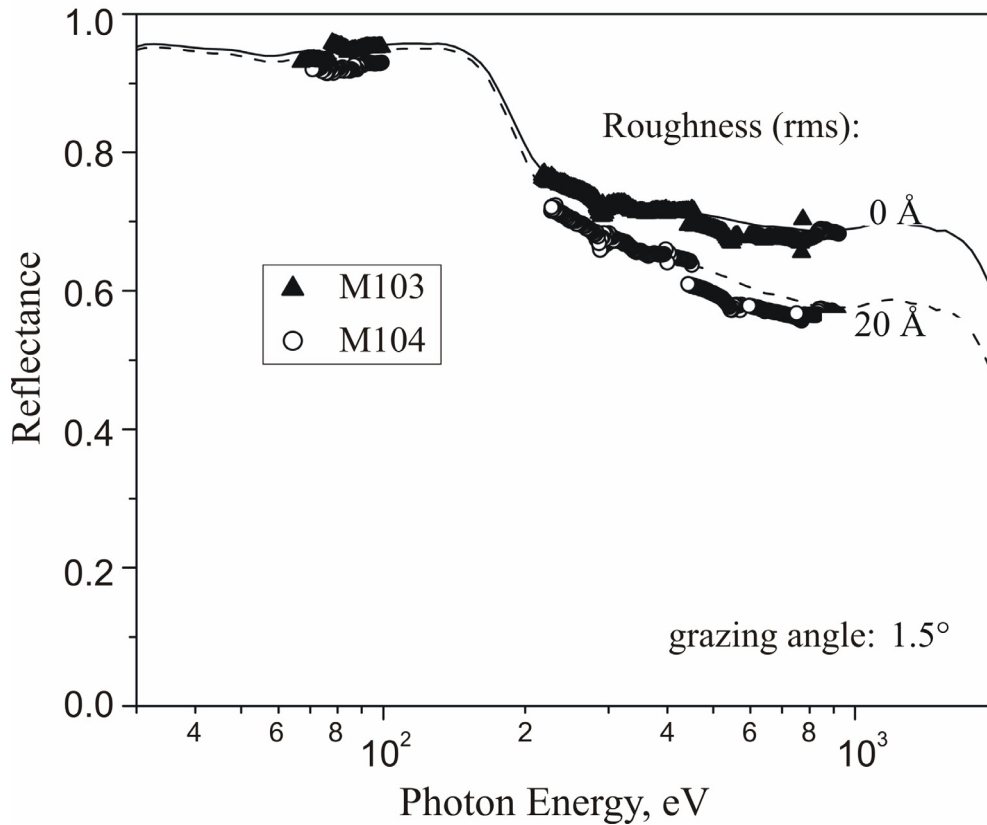
Figure 10: X-ray energy dependences of the surface reflectance measured with the nickel coated steel mirror (the open points) the M104 directly polished stainless steel mirror (the filled points). The solid and the dashed lines represent the theoretical spectra computed from tabulated optical properties of gold, with a Nevot-Croce treatment of the loss due to surface roughness assuming the mirror surface roughness of 5 Å for the nickel coated steel mirror M103 and 20 Å for the directly polished stainless steel mirror, M104. The steel reflectivity is reduced above 200eV by surface roughness effects.
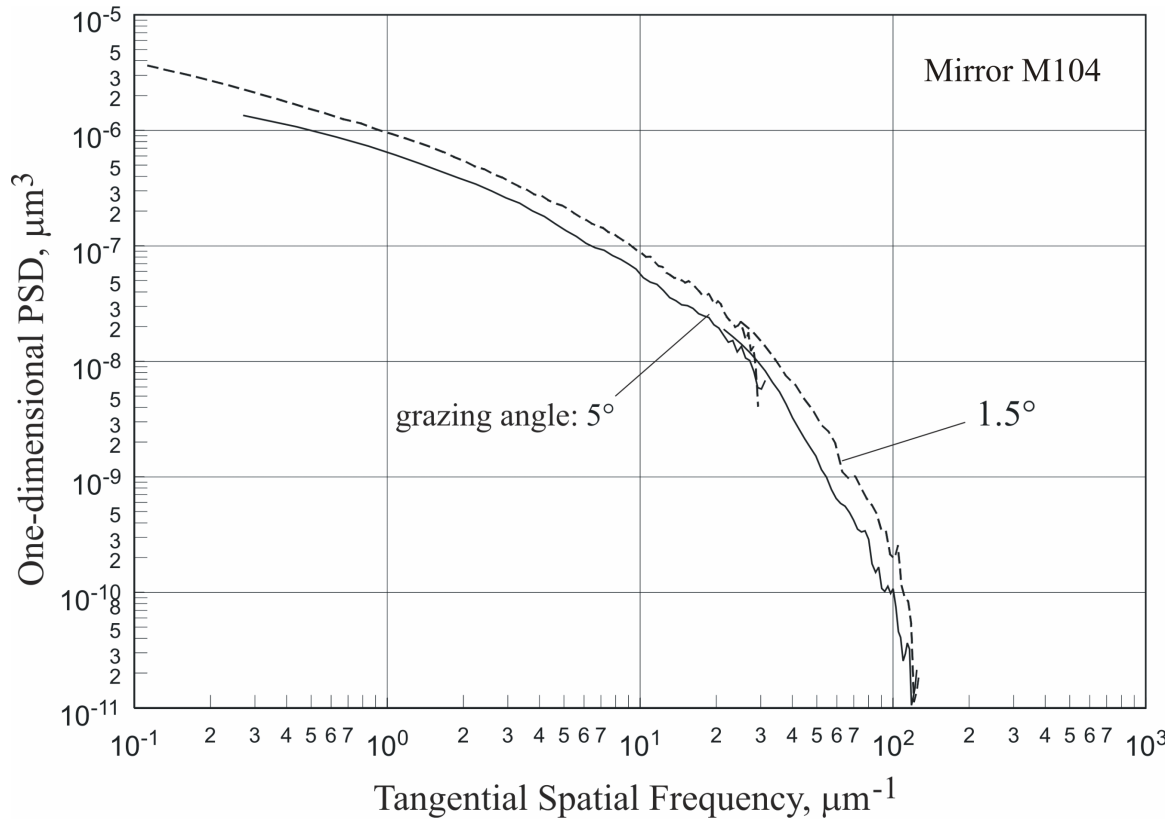
Figure 11: The 1D PSD spectra extracted from the X-ray scattering measurements with the M104 directly polished mirror. The solid line corresponds to the X-ray beam grazing incidence angle of 1.5°; and the dashed line obtained at the beam grazing angle of 5°. The measurements were performed at photon energy of 92 eV.
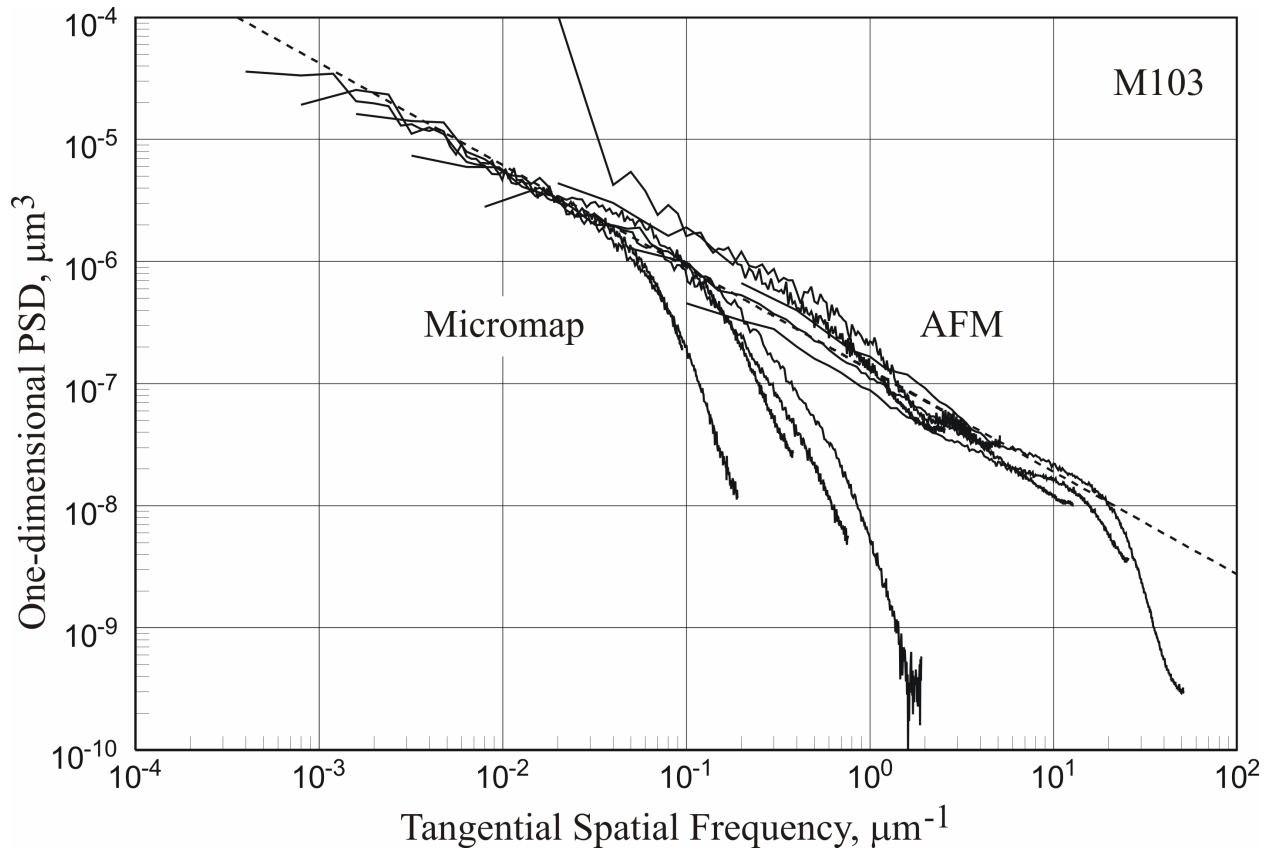
Figure 12: Tangential 1D PSD spectra obtained with the M103 nickel coated mirror. The spectra at lower spatial frequencies show the measurements with different objectives of the interferometric microscope (compare with Fig. 4); the spectra at higher spatial frequencies represent the Atomic Force Microscope data (compare with Fig. 7). The dashed line represents an inverse-power-low spectrum, enveloping all the measured spectra. Note that the parameters of inverse-power-low spectrum (Table 3) are the same as for the sagittal 1D PSD spectra measured with the Micromap and AFM.
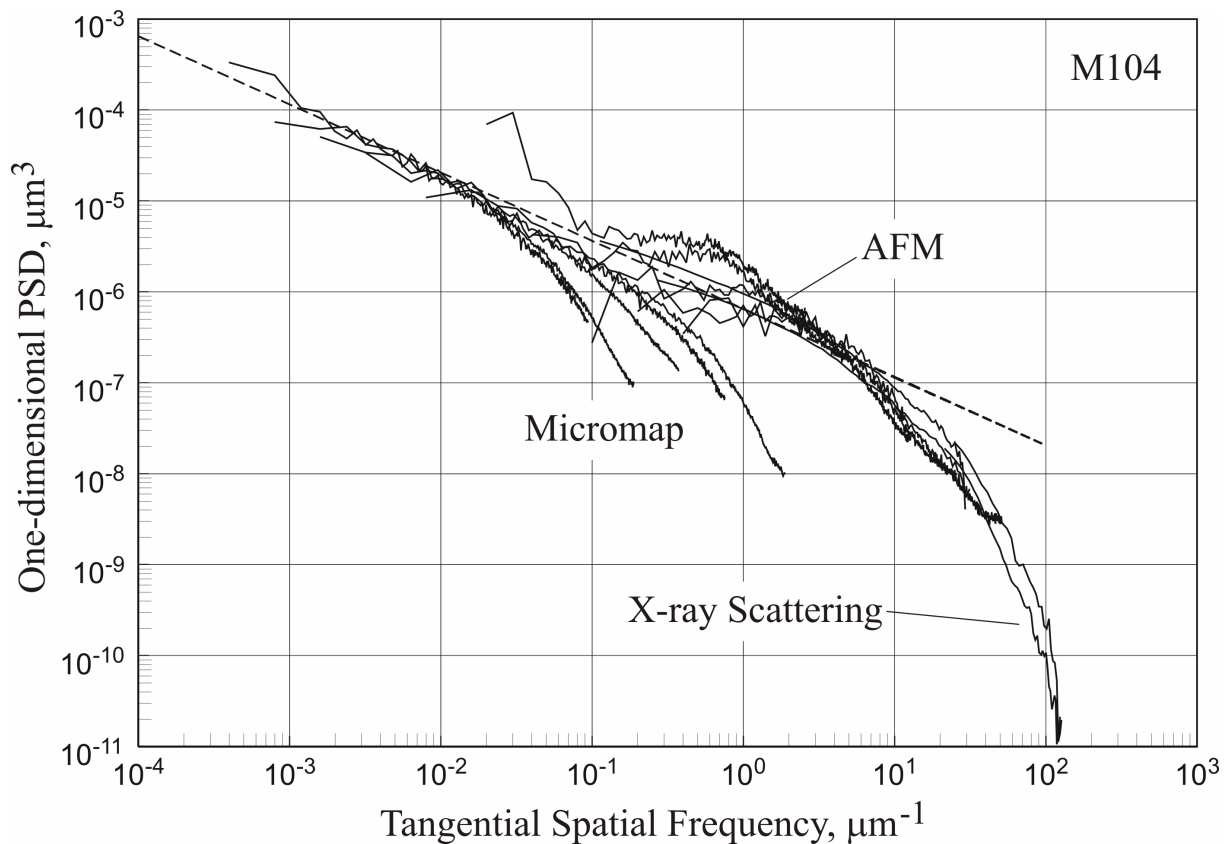
Figure 13: Tangential 1D PSD spectra obtained with the directly polished stainless steel mirror M104. The spectra at lower spatial frequencies show the measurements with different objectives of the interferometric microscope (compare with Fig. 5); the spectra at the middle spatial frequencies represent the Atomic Force Microscope data (compare with Fig. 8); the spectra extracted from the X-ray Scattering measurements cover the higher frequencies available. The dashed line represents an inverse-power-low spectrum, enveloping all the measured spectra. Note that the parameters of the inverse-power-low spectrum (Table 3) are the same as for the sagittal 1D PSD spectra measured with the Micromap and AFM.

Tables

Tables 1. The Micromap-570 measurements of the rms surface roughness of the three mirrors.

S_q rms (Å)	2.5× objective	5× objective	10× objective	20× objective	100× objective
M103,[a] nickel coated steel mirror	5.3	5.1	7.3	5.4	5.7
M104, steel mirror polished directly	11.2	9.7	13.5	19.2	17.4
M105, steel mirror polished directly	9.6	10.8	13.1	17.2	13.7

---

[a] Here we keep the mirror labeling used on the corresponding ALS beamline.

Table 2. The AFM measurements of the surface roughness (rms) of two of the mirrors.

S_q rms (Å)	5×5 μm² area	10×10 μm² area	20×20 μm² area	50×50 μm² area	100×100 μm² area
M103, nickel coated steel mirror	6.8	6.4	6.2	9.2	15.7
M104, steel mirror polished directly	16.4	15.3	14.9	14.2	18.0

Table 3. Measured power-law parameters obtained for the frequency range from approximately $3 \cdot 10^{-4}$ μm^{-1} to 10 μm^{-1} and corresponding roughness calculated over frequency range characteristic for the 5× objective.

	Spectral intensity, $S_1(1)$	Spectral index, γ	Roughness (rms), S_q (Å)
M103, nickel coated steel mirror	$1.3 \cdot 10^{-7}$	0.838	6.4
M104, steel mirror polished directly	$6.5 \cdot 10^{-7}$	0.75	10.8
M105, steel mirror polished directly	$5.5 \cdot 10^{-7}$	0.83	13.0